

RESEARCH ARTICLE | AUGUST 04 2023

Gate-tunable resistance drops related to local superconducting gaps in thin TaS₂ layers on SrTiO₃ substrates

M. Kosugi; R. Obata; K. Suzuki; K. Kuroyama ; S. Du; B. Skinner ; T. Kikkawa ; T. Yokouchi; Y. Shiomi ; S. Maruyama ; K. Hirakawa ; E. Saitoh ; J. Haruyama  

 Check for updates

APL Mater 11, 081106 (2023)

<https://doi.org/10.1063/5.0147818>

 CHORUS


View
Online


Export
Citation

CrossMark



THE ADVANCED MATERIALS MANUFACTURER®

Li	Be	B	C	N	O	F	Ne										
Na	Mg	Al	Si	P	S	Cl	Ar										
K	Ca	Sc	Ti	V	Cr	Mn	Fe	Co	Ni	Cu	Zn	Ga	Ge	As	Se	Br	Kr
Rb	Sr	Y	Zr	Nb	Mo	Tc	Ru	Rh	Pd	Ag	Cd	In	Sn	Sb	Te	I	Xe
Cs	Ba	La	Hf	Ta	W	Re	Os	Ir	Pt	Au	Hg	Tl	Pb	Bi	Po	At	Rn
Fr	Ra	Ac	Rf	Db	Sg	Bh	Hs	Mt	Ds	Rg	Cn	Nh	Fl	Mc	Lv	Ts	Og
		Ce	Pr	Nd	Pm	Sm	Eu	Gd	Tb	Dy	Ho	Er	Tm	Yb	Lu		
		Th	Pa	U	Np	Pu	Am	Cm	Bk	Cf	Es	Fm	Md	No	Lr		

The Next Generation of Material Science Catalogs

yttrium iron garnet glassy carbon beamsplitters fused quartz additive manufacturing

zeolites III-IV semiconductors gallium lump copper nanoparticles organometallics

nano ribbons barium fluoride europium phosphors photonics infrared dyes

epitaxial crystal growth ultra high purity materials transparent ceramics CIGS

sapphire windows Nd:YAG cerium oxide polishing powder cermet nanodispersions

spintronics raman substrates surface functionalized nanoparticles MBE grade materials thin film

silver nanoparticles perovskites OLED lighting solar energy

MOCVD beta-barium borate sputtering targets fiber optics

rare earth metals quantum dots h-BN deposition slugs

osmium scintillation Ce:YAG CVD precursors photovoltaics

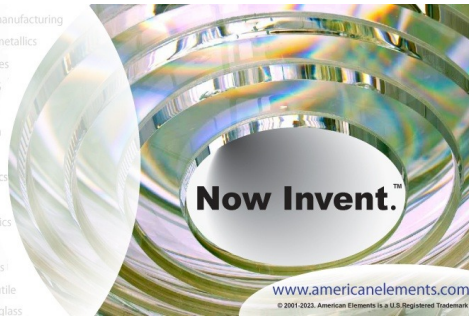
refractory metals laser crystals refractory metals laser crystals

anodic aluminum oxide niobate InAs wafers metamaterials borosilicate glass

ZnS CdTe MOFs AuNPs YBCO superconductors InGaAs

perovskite crystals transparent ceramics indium tin oxide MgF₂ rutile optical glass

diamond micropowder



Now Invent.™

www.americanelements.com

© 2001-2022, American Elements LLC, a U.S. Registered Trademark

Gate-tunable resistance drops related to local superconducting gaps in thin TaS₂ layers on SrTiO₃ substrates

Cite as: APL Mater. 11, 081106 (2023); doi: 10.1063/5.0147818

Submitted: 31 March 2023 • Accepted: 17 July 2023 •

Published Online: 4 August 2023



View Online



Export Citation



CrossMark

M. Kosugi,¹ R. Obata,¹ K. Suzuki,¹ K. Kuroyama,² S. Du,² B. Skinner,³ T. Kikkawa,⁴ T. Yokouchi,⁵ Y. Shiomi,⁵ S. Maruyama,⁶ K. Hirakawa,² E. Saitoh,^{4,7,8,9} and J. Haruyama^{1,2,a)}

AFFILIATIONS

¹ Faculty of Science and Engineering, Aoyama Gakuin University, 5-10-1 Fuchinobe, Sagamihara, Kanagawa 252-5258, Japan

² Institute for Industrial Sciences, The University of Tokyo, 4-6-1 Komaba, Meguro-ku, Tokyo 153-8505, Japan

³ Department of Physics, The Ohio State University, Columbus, Ohio 43202, USA

⁴ Department of Applied Physics, The University of Tokyo, 7-3-1 Hongo, Bunkyo-ku, Tokyo 113-8656, Japan

⁵ Department of Basic Science, The University of Tokyo, 3-6-1 Komaba, Meguro-ku, Tokyo 153-8902, Japan

⁶ Department of Mechanical Engineering, The University of Tokyo, 7-3-1 Hongo, Bunkyo-ku, Tokyo 113-8656, Japan

⁷ Institute for AI and Beyond, The University of Tokyo, 7-3-1 Hongo, Bunkyo-ku, Tokyo 113-8656, Japan

⁸ WPI Advanced Institute for Materials Research, Tohoku University, 2-1-1 Katahira, Aoba-ku, Sendai 980-8577, Japan

⁹ Advanced Science Research Center, Japan Atomic Energy Agency, 2-4 Shirakata, Tokai-mura, Naka-gun, Ibaraki 319-1195, Japan

^{a)} Author to whom correspondence should be addressed: J-haru@ee.aoyama.ac.jp

ABSTRACT

Strontium titanate [SrTiO₃ (STO)], a perovskite oxide with an extremely high gate-tunable dielectric constant (ϵ) due to quantum paraelectric phases, is attracting considerable attention for yielding various physical phenomena when two-dimensional (2D) layers are integrated. Superconductivity is such a typical phenomenon. However, the influence of the STO substrates on enhancing transition temperatures (T_c) for (atomically) thin 2D flakes attached to them has been rarely investigated. Here, we report gate-tunable and gradual four-terminal resistance drops with critical onset T (T_{CR}) and scanning tunneling spectroscopy (STS) spectra in devices comprising thin TaS₂ flakes attached on monolayer hexagonal boron nitride (hBN) spacer/STO substrates. Observation of STS spectra confirms the presence of local superconducting gaps Δ (~ 1.5 meV) with transition T ($T_{\Delta C}$) three-times higher than previous reports of T_c under absent pressure and strong position dependence of Δ . Depending on Δ on back gate voltages (V_{bg}) and magnetic fields, there is a strong correlation between T_{CR} and the onset T_c of superconductivity, implying an enhancement of approximately five times compared with the previous highest-onset T_c values without pressure as the applied V_{bg} increases. The high onset T_c and Δ are discussed based on screening of the long-range Coulomb interaction (CI) due to the high- ϵ of SrTiO₃, while the short-ranged CI remains strong in the 2D limit, causing the superconductivity. Using a monolayer hBN/SrTiO₃ substrate with V_{bg} opens doors to T_c enhancement in thin superconducting layers integrated on it and wide application due to the solid-state high- ϵ substrates.

© 2023 Author(s). All article content, except where otherwise noted, is licensed under a Creative Commons Attribution (CC BY) license (<http://creativecommons.org/licenses/by/4.0/>). <https://doi.org/10.1063/5.0147818>

I. INTRODUCTION

Strontium titanate [SrTiO₃ (STO)],^{1–8} a perovskite oxide with quantum paraelectric phases at low temperature (T), is attracting considerable attention because of (1) an anomalously large and back gate-voltage (V_{bg}) tunable dielectric constant (e.g., $\epsilon \sim 10^4$ at $T = 2$ K) through all T regimes due to strong quantum fluctuation^{1–3} and (2) specified surface states.^{5,6} These create abundant high- T physical phenomena, such as high transition temperatures (T_c) superconductivity, novel quantum Hall states (quantum Hall topological insulators), and Majorana zero-bias states^{1–8} (the supplementary material, 1), which arise from the introduction of (1) the high charge carrier density n_D and (2) the unique two-dimensional (2D) electronic states into the interfaced materials, respectively. Among those, high- T_c superconductivity is of great interest because of the discovery of T_c [owing to (2)] as high as ~ 100 K in mono-atom layer FeSe directly grown on the STO substrate.⁵ However, the influence of the STO substrates on enhancing T_c for (atomically) thin 2D flakes, which are mechanically exfoliated and attached to the substrates, has been rarely investigated.

On the other hand, superconductivity in various (atomically) thin 2D layers, which were mechanically exfoliated and attached to a silicon oxide (SiO₂)/silicon substrate, has been widely researched from many perspectives.^{9–20} Enhancement of T_c depends on a number of physical factors, such as n_D , layer number (the thickness d), and in-plane or interlayer Coulomb interaction (CI).

The thin transition metal dichalcogenide (TMDC), titanium disulfide (TaS₂), exhibits such superconducting characteristics in both its 1T- and 2H-phases, indirectly competing with charge density wave (CDW) states depending on n_D .^{9–13} For instance, T_c increased up to 2 K as d decreased to ~ 3 nm from ~ 15 nm (bulk with $T_c \sim 0.7$ K) in conventional non-doped 2H structures without applying V_{bg} .⁹ Because the interlayer CI is weak, the T_c was enhanced by increasing the 2D electronic density of states (EDOS), which is caused by the growth of a van Hove singularity (vHS) driven by in-plane strong repulsive CI [i.e., Luttinger liquid (LL) states] and the alignment of the Fermi level (E_F) with the vHS.^{19,21,31–33} Moreover, a significant increase in T_c up to 8.5 K was observed in 2H-TaS₂ when a pressure of 9.5 GPa was applied.³⁴

In contrast, gate-controlled Li-ion heavy intercalation into the 1T structure demonstrated contradictory results, i.e., T_c (~ 2 K) decreased with decreasing d and the superconducting phase finally disappeared at $d \sim 3$ nm, whereas nearly commensurate CDW and Mott insulating phases became dominant.²⁰ This situation is analogous to the case of Bardeen–Cooper–Schrieffer (BCS) superconductivity in systems with strong interlayer coupling, such as NbSe₂^{14–16} and heavily doped MoS₂ (Ising superconductivity).^{17,18}

Without applying pressure, in all cases, the maximum (onset) T_c in TaS₂ flakes attached to SiO₂/Si substrates was limited below ~ 2 K, except for some specified cases.^{11,12} In particular, the influence of the substrates on enhancing T_c has been rarely investigated, even for the STO substrate.

II. EXPERIMENTAL

A. Sample preparation and characterization

In the present experiment, thin 1T-TaS₂ flakes were attached to a mono-layer hexagonal boron nitride (hBN) spacer atop an

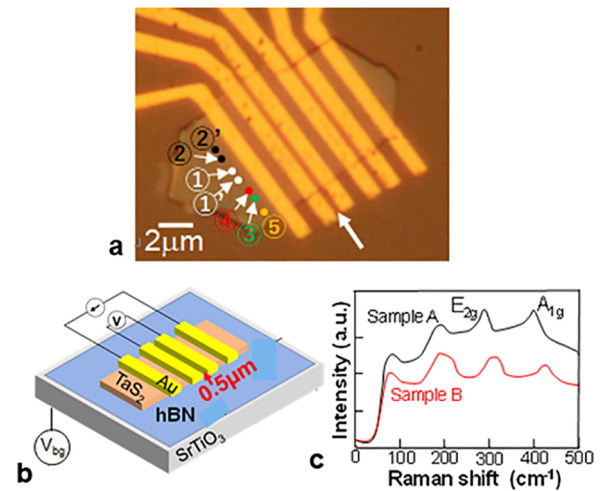


FIG. 1. (a) AFM images of 1T-TaS₂ flake/monolayer hBN/STO substrate (the supplementary material, 2) with four terminal Au/Ti electrodes; the interelectrode spacing of 500 nm is used for R measurements (indicated by the white arrow). The numbers ①–⑤ indicate the positions used for the observation of STS spectra. (b) Schematic overview of a part of (a) with V_{bg} connection to the back side of the STO substrate. (c) Room-temperature Raman spectra for samples A and B with thicknesses of ~ 8 and ~ 3 nm, respectively.

STO substrate [Figs. 1(a)–1(c)] (Methods and the supplementary material, 2). The thickness d of TaS₂ flakes was confirmed by Raman spectroscopy [via E_{2g} and A_{1g} peaks in Fig. 1(c)] and atomic force microscopy (AFM) (the supplementary material, 2). The STO substrates used here have large surface roughness at some points, which may lead to non-zero resistance (R) at $T = 2$ K, as shown later (the supplementary material, 2). Four-terminal Au/Ti electrodes with 500 nm space between two electrodes for R observation [e.g., white arrow in Fig. 1(a)] were formed on the flakes using conventional electron-beam lithography methods to detect the small superconducting area [Fig. 1(b)] (the supplementary material, 3). Before electrode evaporation, the surface of TaS₂ was slightly etched by the Ar ion to avoid the influence of oxidation. Four-terminal R as functions of T , V_{bg} , and out-of-plane magnetic fields (B) were measured by Dyna Cool (Quantum Design) using a lock-in amplifier, applying V_{bg} from the back side of the STO substrate [Fig. 1(b)], without applying pressure. Positions used for observation of scanning tunneling spectroscopy (STS) spectra are shown in the numbers ①–⑤.

B. Observation of four-terminal resistance drops

Figure 2(a) shows the four-terminal R of a sample with $d \sim 8$ nm (sample A) as a function of T (i.e., from a T of 300–2 K) with $V_{bg} = +30$ V and $B = 0$. As T decreases, R monotonically decreases and abruptly drops below critical T (T_{CR}) ~ 10 K (shown in the red arrow). Figure 2(b) presents the V_{bg} dependence of the R – T feature shown in Fig. 2(a). This figure reveals an accurate T_{CR} of ~ 3.8 K at $V_{bg} = 0$ V (shown in the red arrow) and its shift to a higher T with increasing V_{bg} (i.e., to a T_{CR} of ~ 6 K at $V_{bg} = +40$ V).

In contrast, Fig. 2(c) demonstrates a similar dependence in sample B with a smaller thickness ($d \sim 3$ nm). It also implies the

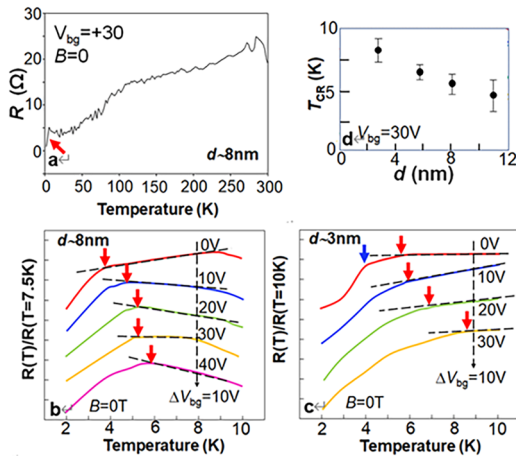


FIG. 2. (a) R - T relationship of sample A up to room temperature. The red arrow indicates an abrupt R drop below $T = 10$ K. (b) V_{bg} dependence of the R - T feature in sample A [shown in Fig. 2(a)] and (c) sample B with $d \sim 3$ nm. The dotted lines are just a guide for the eyes, and the red arrows are critical temperatures for R drops (T_{CR}). The blue arrow in c means the lower case of T_{CR} . Because applying a larger V_{bg} electrostatically destroys TaS₂ layers, V_{bg} was limited below +40 and +30 V for (b) and (c), respectively. (d) T_{CR} as a function of d , including the results in (b) and (c) at $V_{bg} = +30$ V. The error bars mean the measurement results of three samples in each d .

evident $T_{CR} \sim 5.8$ K at $V_{bg} = 0$ V (red arrow) with the second abrupt R drop at $T_{CR} \sim 4$ K (blue arrow), which increases as V_{bg} increases, resulting in the highest $T_{CR} \sim 9$ K at $V_{bg} = +30$ V. The T_{CR} values are higher than those in Fig. 2(b) at individual values of V_{bg} . The normalized R value drops by a factor of four from the T_{CR} to $T = 2$ K at $V_{bg} = +30$ V. The T_{CR} as a function of d , including the results in Figs. 2(c) and 2(d) at $V_{bg} = +30$ V, is demonstrated in Fig. 2(d). It is clear that the T_{CR} monotonically increases with decreasing d . When the T_{CR} values are compared with the onset T_c for superconductivity in (atomically)thin TaS₂, the highest T_{CR} values of ~ 6 K (sample A) and ~ 9 K (sample B) are approximately three and five times higher than the highest onset T_c of 2 K without pressure.^{9,10} They are also larger than those even in highly disordered (~ 4 K) or oxygenated (~ 3 K) TaS₂.^{11,12}

C. STS spectra confirming local superconducting gaps

Here, the R drops are gradual below the T_{CR} , with non-zero R values at $T = 2$ K. In order to confirm the origin, STS spectra have been measured at seven local points of flake B [Fig. 1(a) and the supplementary material, 4]. The results are shown in Fig. 3. The T -dependence of dI/dV vs V is shown for $V_{bg} = +30$ V at the local position ①, which is one of the positions exhibiting Δ [①, ①', ③-⑤ in Fig. 1(a)], in Fig. 3(a). The dI/dV gap Δ starts to appear at $T = 10$ K and increases as T decreases, resulting in the entire Δ reaching 0 Ω at $T_{\Delta C} = 6$ K and the $\Delta \sim 0.4$ mV with smearing at $T = 2$ K. V_{bg} and position dependence of Δ at $T = 2$ K are shown in Fig. 3(c). $\Delta \sim 1$ and ~ 0.1 mV for $V_{bg} = +30$ and 0 V, respectively, can be confirmed at the local position ①. The dependence of Δ at $T = 2$ K on perpendicular magnetic fields (B_{\perp}) is shown in Fig. 3(d). The magnitude of Δ decreases with increasing B_{\perp} (particularly

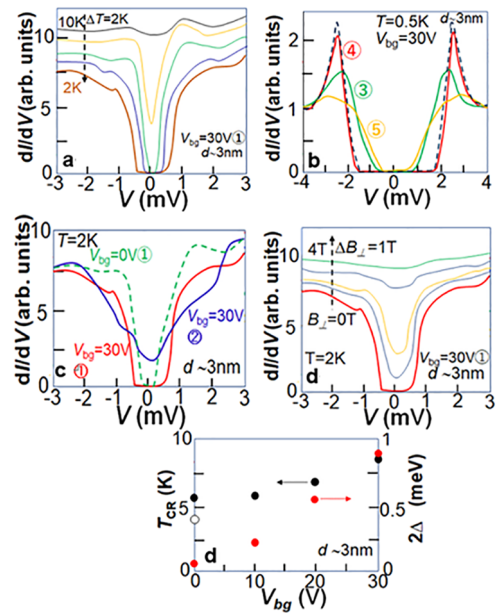


FIG. 3. Scanning tunneling spectroscopy (STS) spectra [corresponding to the positions shown in Fig. 1(a) and measured by $V = 0.05$ V, $I = 2.0$ nA] (the supplementary material, 4) observed at (a) position ① for different T (> 2 K) under a fixed V_{bg} , at (b) positions ③-⑤ at $T = 0.5$ K (being normalized by dI/dV at $V = \pm 4$ mV), (c) two different positions ① and ② (~ 200 nm distance), and (d) B_{\perp} dependence of (a) at $T = 2$ K. At position ①, two different V_{bg} are employed. The dotted curve in (b) is the superconducting gap fitted with the Dynes model [Eq. (1)]. (e) T_{CR} and Δ at $T = 2$ K (filled black and red circles, respectively) as a function of V_{bg} , including the results in Figs. 2(c) and 3(c) [i.e., red arrows in Fig. 2(c) and position ① in Fig. 3(c)]. The open circle corresponds to the blue arrow in Fig. 2(c).

from 2 T) and disappears around $B_{\perp} = 4$ T. These behaviors are in qualitatively good agreement with those in previous reports of superconductivity in TaS₂, and, thus, suggest that the observed Δ corresponds to the local superconducting gaps.

In order to reconfirm superconductivity, STS measurements at $T < 2$ K (i.e., $T = 0.5$ K) were carried out at the other three positions ③-⑤ [Fig. 1(a)], and data fit was performed by the Dynes model [Eq. (1)] for conventional superconductivity.^{22,23} The results are shown in Fig. 3(b) (normalized by dI/dV at $V = \pm 4$ mV). Although Δ values and shapes highly depend on the positions, position ④ demonstrates the largest Δ value of ~ 1.5 meV with suppressed thermal smearing. The data fit shows the best agreement with the observed curve when the fitting parameters $\Delta \sim 1.5$ meV and the pair breaking parameter $\Gamma \sim 5 \times 10^{-3}$ are employed.

$$N(\omega) = N_0 \operatorname{Re} \left[\frac{\omega + i\Gamma}{(\omega + i\Gamma)^2 - \Delta^2} \right], \tag{1}$$

where $N(\omega)$ is the tunneling density of states, Γ is the effect of the pair-breaking processes, and N_0 is the normal-state density of states at the Fermi level. This result is discussed in detail in the discussion section later.

The $T_{\Delta C} = 6$ K in Fig. 3(a) is also at least three times higher than previous reports of the T_c in TaS₂ under no pressure. Reduction of the Δ values from $V_{bg} = 30-0$ V qualitatively agrees with those in the

T_{CR} [Fig. 3(e)]. This also implies the strong correlation of the T_{CR} with the onset T_c .

In contrast, Δ disappears at different positions ② and ②', where it is located ~ 200 nm away from ① [Figs. 1(a) and 3(c)]. We confirmed such strong position dependence of Δ at seven random points as mentioned above. This result suggests that one of the main reasons for the non-zero R drops is a non-uniform and local superconducting transition owing to the large local-roughness of the STO surface (the supplementary material, 2) or strain. It obstructs the appearance of the homogeneous superconducting transition (arising from the screening of CI as discussed later) over entire parts between the two electrodes (within a 500 nm distance) used for the R measurements [Fig. 1(b)].^{24,25} Because the superconducting regions with Δ only locally emerge such as islands and cannot connect the two electrodes at $T = 2$ K, the non-superconducting regions obstruct the appearance of the R drop down to 0Ω .

D. V_{bg} and B dependence of resistances

Figures 4(a) and 4(b) show R vs V_{bg} relationships for different T at $B = 0$ T in sample B (the supplementary material, 5). R increases as V_{bg} decreases in the $+V_{bg}$ region for all T regions in Fig. 4(b). For $+V_{bg} > \sim 3$ V, R monotonically decreases with a decrease in T , whereas for $+V_{bg} < \sim 3$ V, R becomes insensitive to T change at $T > 4$ K as $+V_{bg}$ decreases and becomes almost constant, resulting in the largest R drop between $T = 3$ and 4 K. These results are in good agreement with those shown in Fig. 2(d), which showed a decrease in the onset T_c in the lower V_{bg} region. In contrast, the T dependence of the R vs V_{bg} relationships suggests transitions to the possible CDW phase (the supplementary material, 6) in the $-V_{bg}$ region, particularly at $V_{bg} < \sim -7$ V [Fig. 4(a)].

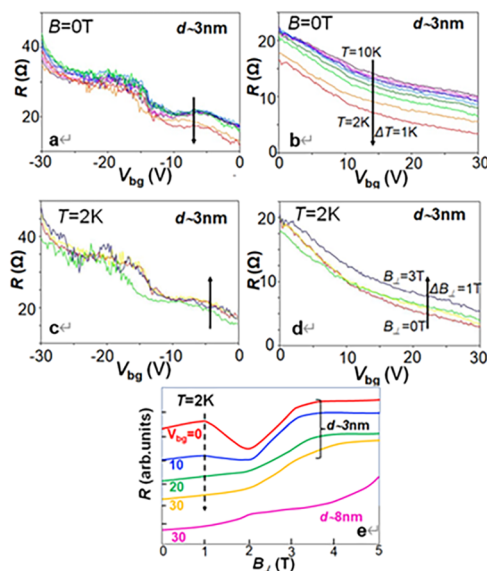


FIG. 4. Four-terminal R measurements as functions of V_{bg} for (a) and (b) different T and (c) and (d) different B_{\perp} applied perpendicular to the sample plane in sample B (the supplementary material, 5). (e) R vs B_{\perp} relationships at each V_{bg} of (d), including that for $V_{bg} = +30$ V in sample A.

Figures 4(c) and 4(d) demonstrate the R vs V_{bg} relationships for different B_{\perp} at $T = 2$ K in sample B (the supplementary material, 5). In Fig. 4(c), R values monotonically increase for all B_{\perp} with decreasing V_{bg} , whereas the B_{\perp} dependence of R reveals a different tendency around $V_{bg} \sim 10$ V in the $+V_{bg}$ region. At $V_{bg} > \sim 10$ V, R monotonically increases as B_{\perp} increases, whereas R values at $B_{\perp} = 0$ and 2 T become the highest and smallest values, respectively, except for the R at $B_{\perp} = 3$ T at $V_{bg} < \sim 10$ V. For the $-V_{bg}$ region in Fig. 4(c), these R tendencies are still maintained, although the B_{\perp} dependence becomes much weaker except for the R value at $B_{\perp} = 2$ T (the supplementary material, 6).

R vs B_{\perp} relationships at $T = 2$ K in sample B are shown for the $V_{bg} = 0$ V and $+V_{bg}$ regions in Fig. 4(e), including that for $V_{bg} = +30$ V shown in sample A. R values monotonically and gradually increase with increasing B_{\perp} and drastically increase above $B_{\perp} \sim 2$ T for $V_{bg} = 10$ –30 V. They saturate at $B_{\perp} \sim 4$ T. These results are in qualitatively good agreement with those in Fig. 3(b), suggesting a close correlation with superconductivity. On the other hand, R at $V_{bg} = 0$ V shows quite different behavior due to the influence of the CDW.

E. Discussion

We have shown the observation of the gradual R decrease starting from T_{CR} with decreasing T and resulting in a non-zero value at $T = 2$ K (Fig. 2) and the corresponding local STS signals Δ (Fig. 3). As shown in Fig. 3(b), the calculation result for Δ using the Dynes model [Eq. (1)] was in good agreement with the observed STS result at $T = 0.5$ K, with the best fitting values for $\Delta \sim 1.5$ meV and $\Gamma \sim 5 \times 10^{-2}$. The value of $\Delta \sim 1.5$ meV corresponds to $T_c \sim 10$ K through $2\Delta/k_B T_c = 3.5$ for the conventional gap equation for superconductivity. Because this $T_c \sim 10$ K value is in good agreement with $T_{CR} \sim 9$ K at $V_{bg} = +30$ V in Fig. 3, it implies a strong possibility that T_{CR} can be the onset T_c . This result means that R cannot abruptly drop to 0Ω over the entire area between the electrodes, even when the local Δ opens in the present material. The gradual R drops with decreasing T reflect just the gradual R decrease due to the metallic conductivity in the area outside the local points with Δ . The best fitting parameter $\Gamma \sim 5 \times 10^{-2}$ also indicates that geometrical factors (e.g., disorder, oxidation), which introduce a large Γ , are not large in some positions of the present TaS₂ flakes.

As possible origins for the gradual R drops other than superconductivity, charge fluctuation originating from the STO substrate with high dependence on V_{bg} might be the most probable, because such gradual R drops starting from a high T regime were not observed in our TaS₂ flakes attached to a SiO₂/Si substrate. Indeed, STO has quantum fluctuations in the low T region, as mentioned in the introduction. However, because it does not lead to the observed local Δ in STS, it is not associated with the gradual R drops. Thus, superconductivity has one of the highest possibilities.

Based on this, we discuss the correlation of superconductivity with the observed onset of T_c (i.e., T_{CR}) enhancement. One of the origins of this TaS₂ superconductivity on SiO₂/Si substrates could be the growth of a vHS driven by in-plane strong repulsive CI and the alignment of E_F with it by decreasing d to the 2D limit^{9,19} (the supplementary material, 7). This mechanism can qualitatively correspond to the present case because T_c increases with decreasing d . Moreover, the work, which reported the significant

increase in T_c up to 8.5 K in 2H-TaS₂ under a pressure of 9.5 GPa,³⁴ also found that, unexpectedly, CDW and superconductivity could coexist in a large part of the phase diagram when applying pressure. Although observation of such an interaction between CDW and superconductivity is highly interesting in the present system because our samples have a similar onset T_c despite applying no pressure, the two regimes have been distinctly separated by applying V_{bg} in the present samples using the STO substrate with a high ϵ . CDW might be caused only in the $-V_{bg}$ region via hole doping in this case. Thus, the comparison is difficult.

In addition to this repulsive-CI based model, the much higher onset T_c observed in the present structure can originate from the large ϵ of the STO substrate, i.e., (1) the large n_D doping by applying V_{bg} to the high- ϵ STO substrate and (2) screening of the long-range CI by the high n_D . The first term is analogous to that in the gate-controlled Li-ion heavy intercalation into 1T-TaS₂.¹⁰ In the present case, applying large V_{bg} to the high- ϵ STO substrate dopes large n_D into the thin TaS₂. Indeed, the estimated $n_{2D} \sim 10^{14} \text{ cm}^{-2}$ at $V_{bg} = +30 \text{ V}$ and $T = 2 \text{ K}$ in sample B is almost equivalent to the lowest case of an extremely large n_{2D} of the Li-ion intercalated 1T-TaS₂. However, the onset T_c was still below 2 K even at $n_{2D} > \sim 2 \times 10^{14}$ in the Li-doped TaS₂, while the present onset- T_c is much higher than 2 K. Thus, the second term becomes important as follows:

Enhancement of superconductivity by screening of the long-range CI was reported as a model to explain the appearance of the superconductivity in heavily doped MoS₂ layers.¹⁷ The superconductivity was mediated by the short-range, intermittently repulsive CI. When it is assumed that the long-range CI was strongly screened by the high n_{2D} , which was brought about by heavy doping via the ionic-liquid gate, the effect of the short-range repulsive CI was enhanced, resulting in the emergence of superconductivity. A similar mechanism can work in our devices since the long-ranged part of the CI between electrons in TaS₂ is effectively screened by the large ϵ of the STO substrate.²⁶

Indeed, the long-range CI was screened by the large ϵ of the STO substrate in the graphene/few-layer hBN/STO substrate, resulting in the appearance of the quantum Hall (QH) topological insulating phase (i.e., a copy of two QH phases)^{4,25,26} (the supplementary material, 1). Although this model¹⁷ was not available for the extremely high n_D region ($> \sim 1.3 \times 10^{14} \text{ cm}^{-2}$) and did not explain the decrease in T_c observed in such regions (e.g., decreasing d) in the heavily doped MoS₂ layers¹⁸ (similar to the cases for the Li-ion intercalated TaS₂¹⁰ and interlayer-coupled NbSe₂^{14–16} mentioned in Sec. I), it is more appropriate for the present results, which show the maximum $n_D < \sim 1 \times 10^{14} \text{ cm}^{-2}$ and the increase in T_c with decreasing d .

We show another estimation of this model as follows: In general, in a conducting 2D electron gas, the long-ranged part of the CI is screened by the Fermi sea, such that at distances $r \gg r_s$, the usual $\sim e^2/\epsilon r$ CI is replaced by the more quickly decaying $\sim e^2 r_s^2/\epsilon r^3$, where r_s is the screening radius. The value of r_s depends inversely on the EDOS ν , as $r_s = 2\pi\epsilon/(e^2\nu)$, so increasing the ν by V_{bg} produces an increasingly prominent truncation of the CI. Naively inserting the large ϵ of STO into the formula for r_s yields a very long r_s , which would be irrelevant at the scale of the electron–electron separation. However, the relevant ϵ is likely to be smaller due to strain and inhomogeneity at the STO surface [Figs. 1(a)–1(c)], which stiffens the transverse optical phonon mode.^{27–29} In this case, the value of r_s may

not be too large, so electronic screening of the long-range CI can be relevant.

Moreover, the short-ranged part of the CI itself may still be relatively large in magnitude due to the dependence of the ϵ on the wave vector q . In particular, the ϵ of STO varies with q as $\epsilon(q) = \epsilon(0)/[1 + (q\xi)^2]$, where $\xi \approx 2.6 \text{ nm}$ (as can be seen by looking at the dispersion of the transverse optical phonon mode in STO³⁰). Consequently, the CI is much larger in magnitude at distances shorter than ξ .

The observed gradual R decreases with the local Δ suggest that this screening of the long-range CI cannot homogeneously emerge between the two electrodes measured, owing to the large surface-roughness of the STO substrate (or strain) (the supplementary material, 2), as T decreases.²⁵ Moreover, the relatively T -independent ϵ of the STO substrate below $T \sim 10 \text{ K}$, due to the softening of ferroelectricity and quantum fluctuations, partially contributes to this mechanism.^{1–3} We also reveal that the monolayer BN spacer plays a definitively important role in addition to the simple physical isolation between the STO and TaS₂ flakes (the supplementary material, 8).

III. CONCLUSIONS

We reported the V_{bg} -tunable gradual four-terminal R drops and STS spectra in thin TaS₂ flakes/monolayer hBN/STO substrates. Observation of the STS spectra confirmed the presence of the local Δ ($\sim 1.5 \text{ meV}$ at $T = 0.5 \text{ K}$) with $T_{\Delta C}$, which is about three-times higher than previous reports of T_c in thin TaS₂ layers under absent pressure, and the strong position dependence of Δ . Its correlation with T_{CR} for V_{bg} and B_{\perp} changes suggested a strong possibility that the observed R drops could be attributed to superconductivity. When the observed T_{RC} corresponds to the onset T_c of superconductivity, it is enhanced approximately five times under the applied V_{bg} , compared with the previous highest-onset T_c values under no pressure. The high onset T_c and Δ were discussed based on screening of the long-range CI due to the high- ϵ of SrTiO₃ with applying V_{bg} .

Further improvement [e.g., using a thinner STO substrate ($\ll 0.5 \text{ mm}$) with a highly uniform surface and no strain] must lead to a full superconducting transition over a large area with a higher T_c . Because of the solid-state and V_{bg} -tunable high- ϵ substrates, the present STO method of attaching mechanically exfoliated thin layers offers the promise of wide application of high- T_c materials.

SUPPLEMENTARY MATERIAL

See the supplementary material for further explanation and experiment details. Fabrication and characterization, STS observation, 3D maps of T vs V_{bg} for R and B vs V_{bg} for R , and result without hBN layer.

ACKNOWLEDGMENTS

We thank K. Otsuka, J. Oka, S. Noda, S. Murakami, K. Nomura, T. Yamamoto, S. Tarucha, T. Ando, T. Enoki, R. Wu, J. J. Palacios, and A. H. MacDonald for their fruitful discussions and encour-

agement. This work performed at Aoyama Gakuin University was supported by the Aoyama Gakuin University Research Institute grant program for the creation of innovative research. The part of work at the University of Tokyo was also supported by JSPS KAKENHI (Grant Nos. JP20H05660, JP19J01737, and JP20K14384 for K.K. and K.H., JP20H02599 for T.K., JP20H00220 for S.M., and JP19H05600 for E.S.), and by JST, CREST (Grant Nos. JPMJCR20B5, Japan for S.M., JP19H05600 and JP20H02599 for E.S.), and the Institute for AI and Beyond of the University of Tokyo for E.S.

AUTHOR DECLARATIONS

Conflict of Interest

The authors have no conflicts to disclose.

Author Contributions

M.K., R.O., K.S., and R.I. fabricated the TaS₂/hBN/STO heterostructure FET and performed all the measurements. K.K. and S.D. supported FET fabrication. T.K., T.Y., and E.S. supported low-*T* measurements. M.K. and J.H. analyzed the data. Y.S., S.M., K.H., and J.H. supervised the project. M.K., B.S., and J.H. wrote the paper with the input of all co-authors.

M. Kosugi: Investigation (equal). **R. Obata:** Investigation (equal). **K. Suzuki:** Investigation (equal). **K. Kuroyama:** Supervision (equal). **S. Du:** Supervision (equal). **B. Skinner:** Supervision (equal); Writing – original draft (equal). **T. Kikkawa:** Supervision (equal). **T. Yokouchi:** Supervision (equal). **Y. Shiomi:** Supervision (equal). **S. Maruyama:** Supervision (equal). **K. Hirakawa:** Supervision (equal). **E. Saitoh:** Supervision (equal). **J. Haruyama:** Project administration (lead); Supervision (lead); Writing – original draft (equal); Writing – review & editing (equal).

DATA AVAILABILITY

The data that support the findings of this study are available within article and its supplementary material.

REFERENCES

- ¹T. Sakudo and H. Unoki, “Dielectric properties of SrTiO₃ at low temperatures,” *Phys. Rev. Lett.* **26**, 851–853 (1971).
- ²D. Shin, S. Latini, C. Schäfer, S. A. Sato, U. De Giovannini, H. Hübener, and A. Rubio, “Quantum paraelectric phase of SrTiO₃ from first principles,” *Phys. Rev. B* **104**, L060103 (2021).
- ³X. He, D. Bansal, B. Winn, S. Chi, L. Boatner, and O. Delaire, “Anharmonic eigenvectors and acoustic phonon disappearance in quantum paraelectric SrTiO₃,” *Phys. Rev. Lett.* **124**, 145901 (2020).
- ⁴L. Veyrat *et al.*, “Helical quantum Hall phase in graphene on SrTiO₃,” *Science* **367**, 781–786 (2020).
- ⁵J.-F. Ge, Z.-L. Liu, C. Liu, C.-L. Gao, D. Qian, Q.-K. Xue, Y. Liu, and J.-F. Jia, “Superconductivity above 100 K in single-layer FeSe films on doped SrTiO₃,” *Nat. Mater.* **14**, 285 (2015).
- ⁶K. Pedersen, S. Ichinokura, T. Tanaka, R. Shimizu, T. Hitosugi, and T. Hirahara, “Interfacial superconductivity in FeSe ultrathin films on SrTiO₃ probed by *in situ* independently driven four-point-probe measurements,” *Phys. Rev. Lett.* **124**, 227002 (2020).

- ⁷C. Chen, K. Jiang, Y. Zhang, C. Liu, Y. Liu, Z. Wang, and J. Wang, “Atomic line defects and zero-energy end states in monolayer Fe(Te,Se) high-temperature superconductors,” *Nat. Phys.* **16**, 536 (2020).
- ⁸S. Das *et al.*, “Observation of room-temperature polar skyrmions,” *Nature* **568**, 368 (2019).
- ⁹E. Navarro-Moratalla *et al.*, “Enhanced superconductivity in atomically thin TaS₂,” *Nat. Commun.* **7**, 11043 (2016).
- ¹⁰Y. Yu *et al.*, “Gate-tunable phase transitions in thin flakes of 1T-TaS₂,” *Nat. Nanotechnol.* **10**, 270 (2015).
- ¹¹J. Peng *et al.*, “Disorder enhanced superconductivity toward TaS₂ monolayer,” *ACS Nano* **12**, 9461–9466 (2018).
- ¹²J. Bekaert *et al.*, “Enhanced superconductivity in few-layer TaS₂ due to healing by oxygenation,” *Nano Lett.* **20**, 3808–3818 (2020).
- ¹³Z. Wang *et al.*, “Surface-limited superconducting phase transition on 1T-TaS₂,” *ACS Nano* **12**, 12619–12628 (2018).
- ¹⁴X. Xi, Z. Wang, W. Zhao, J.-H. Park, K. Law, H. Berger, L. Forró, J. Shan, and K. F. Mak, “Ising pairing in superconducting NbSe₂ atomic layers,” *Nat. Phys.* **12**, 139 (2016).
- ¹⁵H. Wang *et al.*, “High-quality monolayer superconductor NbSe₂ grown by chemical vapour deposition,” *Nat. Commun.* **8**, 394 (2017).
- ¹⁶D. Wickramaratne, S. Khmelevskiy, D. F. Agterberg, and I. I. Mazin, “Ising superconductivity and magnetism in NbSe₂,” *Phys. Rev. X* **10**, 041003 (2020).
- ¹⁷R. Roldan, E. Cappelluti, and F. Guinea, “Interactions and superconductivity in heavily doped MoS₂,” *Phys. Rev. B* **88**, 054515 (2013).
- ¹⁸J. M. Lu, O. Zheliuk, I. Leermakers, N. F. Q. Yuan, U. Zeitler, K. T. Law, and J. T. Ye, “Evidence for two-dimensional Ising superconductivity in gated MoS₂,” *Science* **350**, 1353 (2015).
- ¹⁹Z. Hao *et al.*, “Electric field-tunable superconductivity in alternating-twist magic-angle trilayer graphene,” *Science* **371**, 1133 (2021).
- ²⁰W.-Y. He, B. T. Zhou, J. J. He, N. F. Q. Yuan, T. Zhang, and K. T. Law, “Magnetic field driven nodal topological superconductivity in monolayer transition metal dichalcogenides,” *Commun. Phys.* **1**, 40 (2018).
- ²¹N. Murata *et al.*, “Superconductivity in thin films of boron-doped carbon nanotubes,” *Phys. Rev. Lett.* **101**, 027002 (2008).
- ²²R. C. Dynes *et al.*, “Tunneling study of superconductivity near the metal-insulator transition,” *Phys. Rev. Lett.* **53**, 2437 (1984).
- ²³S. Shen *et al.*, “Coexistence of quasi-two-dimensional superconductivity and tunable Kondo lattice in a van der Waals superconductor,” *Chin. Phys. Lett.* **39**, 077401 (2022).
- ²⁴S. Saha *et al.*, “Unconventional transport through graphene on SrTiO₃: A plausible effect of SrTiO₃ phase-transitions,” *Sci. Rep.* **4**, 6173 (2014).
- ²⁵M. Kosugi *et al.*, “Phase transition between quantum-spin-Hall and quantum-Hall-topological-insulating states in graphene on hBN/SrTiO₃ substrate,” *Nat. Commun.* (submitted).
- ²⁶M. Kharitonov, S. Juergens, and B. Trauzettel, “Interplay of topology and interactions in quantum Hall topological insulators: U(1) symmetry, tunable Luttinger liquid, and interaction-induced phase transitions,” *Phys. Rev. B* **94**, 035146 (2016).
- ²⁷J. M. Worlock and P. A. Fleury, “Electric field dependence of optical-phonon frequencies,” *Phys. Rev. Lett.* **19**, 1176 (1967).
- ²⁸D. Alfè, M. J. Gillan, M. D. Towler, and R. J. Needs, “Diamond and β -tin structures of Si studied with quantum Monte Carlo calculations,” *Phys. Rev. B* **67**, 214102 (2004).
- ²⁹X. X. Xi, A. M. Clark, J. H. Hao, and W. Si, “Dielectric loss of strontium titanate thin films on different substrates,” *Integr. Ferroelectr.* **24**(1–4), 239 (1999).
- ³⁰Y. Yamada and G. Shirane, “Neutron scattering and nature of the soft optical phonon in SrTiO₃,” *J. Phys. Soc. Jpn.* **26**, 396 (1969).
- ³¹P. W. Anderson, “Hall effect in the two-dimensional Luttinger liquid,” *Phys. Rev. Lett.* **67**, 2092 (1991).
- ³²P. W. Anderson, “‘Luttinger-liquid’ behavior of the normal metallic state of the 2D Hubbard model,” *Phys. Rev. Lett.* **64**, 1839–1841 (1990).
- ³³X. Du *et al.*, “Crossed Luttinger liquid hidden in a quasi-two-dimensional material,” *Nat. Phys.* **19**, 40 (2022).
- ³⁴D. C. Freitas *et al.*, “Strong enhancement of superconductivity at high pressures within the charge-density-wave states of 2H-TaS₂ and 2H-TaSe₂,” *Phys. Rev. B* **93**, 184512 (2016).